AGU PUBLICATIONS

JGR

Journal of Geophysical Research: Atmospheres

RESEARCH ARTICLE
10.1002/2017JD026581

Key Points:
- Canopy temperatures around large gaps vary up to 18°C above air temperature during daytime clear-sky conditions
- A correction parameterization was developed to estimate canopy temperatures using air temperature and shortwave radiation
- Mean bias and RMSE could be considerably reduced at 20 radiometer locations during two snowmelt seasons using the new model

Correspondence to:
C. Webster,
clare.webster@northumbria.ac.uk

Citation:
Webster, C., N. Rutter, and T. Jonas (2017), Improving representation of canopy temperatures for modeling subcanopy incoming longwave radiation to the snow surface, *J. Geophys. Res. Atmos.*, *122*, doi:10.1002/2017JD026581.

Received 1 FEB 2017
Accepted 13 AUG 2017
Accepted article online 18 AUG 2017

Improving representation of canopy temperatures for modeling subcanopy incoming longwave radiation to the snow surface

Clare Webster[1,2], Nick Rutter[1], and Tobias Jonas[2]

[1]Department of Geography, School for Engineering and Environment, Northumbria University, Newcastle Upon Tyne, UK, [2]WSL Institute for Snow and Avalanche Research SLF, Davos Dorf, Switzerland

Abstract A comprehensive analysis of canopy surface temperatures was conducted around a small and large gap at a forested alpine site in the Swiss Alps during the 2015 and 2016 snowmelt seasons (March–April). Canopy surface temperatures within the small gap were within 2–3°C of measured reference air temperature. Vertical and horizontal variations in canopy surface temperatures were greatest around the large gap, varying up to 18°C above measured reference air temperature during clear-sky days. Nighttime canopy surface temperatures around the study site were up to 3°C cooler than reference air temperature. These measurements were used to develop a simple parameterization for correcting reference air temperature for elevated canopy surface temperatures during (1) nighttime conditions (subcanopy shortwave radiation is 0 W m^{-2}) and (2) periods of increased subcanopy shortwave radiation >400 W m^{-2} representing penetration of shortwave radiation through the canopy. Subcanopy shortwave and longwave radiation collected at a single point in the subcanopy over a 24 h clear-sky period was used to calculate a nighttime bulk offset of 3°C for scenario 1 and develop a multiple linear regression model for scenario 2 using reference air temperature and subcanopy shortwave radiation to predict canopy surface temperature with a root-mean-square error (RMSE) of 0.7°C. Outside of these two scenarios, reference air temperature was used to predict subcanopy incoming longwave radiation. Modeling at 20 radiometer locations throughout two snowmelt seasons using these parameterizations reduced the mean bias and RMSE to below 10 W m s^{-2} at all locations.

1. Introduction

Boreal and subalpine forests cover much of the Northern Hemisphere and can account for up to 17% of terrestrial water storage through seasonal snow [*Rutter et al*., 2009]. Snowmelt in forested environments contributes substantially to timing and quantity of spring surface runoff, which is strongly controlled by the surface energy budget. The presence of the forest canopy attenuates turbulent energy fluxes, and thus, snowmelt is largely dominated by shortwave and longwave radiations, which can account for up to 92% of the total energy budget available for snowmelt [*Link and Marks*, 1999]. Discontinuous forests with varying canopy densities exhibit the largest spatial and temporal variations in incoming shortwave and longwave radiation, and thus, prediction of the surface radiation budget is most difficult in these forest environments, particularly under high insolation conditions. Heterogeneous forest structures, particularly distinct discontinuities such as gaps and edges, are becoming increasingly prevalent throughout the alpine and boreal environments due to changing land use management practices, forest fires, and climate change. Meter-scale variations in canopy structure and density cause shading of incoming shortwave radiation or exposure of tree stems and trunks to solar heating, resulting in spatial variations in subcanopy radiation different to above-canopy conditions and open environments [*Webster et al*., 2016a]. These discontinuities, however, remain underrepresented in distributed snowmelt models despite their importance in ecohydrological processes.

Canopy heating by absorption of shortwave radiation creates a radiative paradox where decreases in shortwave radiation are often offset by increases in longwave radiation [*Sicart et al*., 2004], which can lead to a net longwave radiation surplus up to 40 W m^{-2} [*Webster et al*., 2016b]. These incoming longwave radiation processes, however, are relatively difficult to predict in discontinuous environments compared to shortwave radiation. Longwave radiation in sun-lit areas of forests has been measured up to 50 W m^{-2} higher than measurements in the shaded edges of gaps, above the canopy or in adjacent open areas [*Lawler and Link*, 2011; *Webster et al*., 2016b]. Forest gaps therefore represent areas with maximum and minimum incoming

longwave radiation to the snow surface, which are strongly dependent on direction of forest exposure in relation to the solar path. Accurate prediction of longwave radiation throughout the subcanopy are important for accurate estimation of snow disappearance date [*Lundquist et al*., 2013], timing of snowmelt for streamflow modeling [*Molotch et al*., 2009], estimations of soil moisture [*Zehe and Blöschl*, 2004], and evapotranspiration rates [*Chen and Zhang*, 1989].

Commonly used methods to estimate subcanopy incoming longwave radiation include using a locally measured air temperature as a proxy for that of the emitting canopy [*Essery et al*., 2008; *Lawler and Link*, 2011; *Sicart et al*., 2004], which can result in errors up to 40 W m^{-2} during sunny clear-sky conditions on exposed canopy edges. Previous studies have demonstrated improvements in incoming longwave radiation prediction by explicitly incorporating either a measured tree trunk temperature [*Webster et al*., 2016b], a canopy shortwave extinction coefficient [*Pomeroy et al*., 2009], a calibrated site-specific linear regression model [*Essery et al*., 2008], or an uncalibrated predetermined relationship between canopy temperature and either air temperature [*Seyednasrollah and Kumar*, 2013] or incoming above-canopy shortwave radiation [*Seyednasrollah and Kumar*, 2014].

Modeling incoming longwave radiation emission from the canopy within forest gaps remains challenging due to the strong heterogeneity of forest structure as well as the lack of availability of forest temperature data, or calibrated methods to estimate this information. Canopy shortwave extinction models or other parameterizations use above-canopy conditions to predict subcanopy incoming longwave radiation based on canopy descriptors such as sky-view fraction (V_f) or effective leaf-area index (LAI′). These methods can work well in closed continuous forest environments when direct solar heating of the canopy is low. For example, *Essery et al*. [2008] used site-calibrated multiple linear regression models with above-canopy conditions as predictor variables and found that estimates of incoming longwave radiation were best in closed canopy environments, and larger errors were found at the forest gap site.

Models thus far are limited in their ability to simply capture variation in exposure of the canopy to direct incoming solar radiation. For example, forest edges or locations on opposite (e.g., north versus south) sides of a gap can have identical above-canopy conditions and V_f or LAI′; however, canopy temperatures in the two environments may differ by up to 20°C depending on the time of day due to exposure direction. This limitation can be overcome through computationally intensive ray-tracing models [e.g., *Musselman et al*., 2015]; however, these are unsuitable over larger forest areas for distributed energy balance and snowmelt models. Development of suitable incoming longwave radiation models for application within distributed snowmelt models have thus far been limited by a lack of distributed canopy surface temperature measurements across forest discontinuities, both spatially and temporally.

Infrared (IR) observations currently represent the most practical means for observing canopy surface temperature variations [*Norman and Becker*, 1995]. The progressive development of infrared thermal imaging technology today allows collection of detailed spatial information regarding temperatures over larger canopy surface areas compared to previously used contact surface measurements [*Pomeroy et al*., 2009; *Webster et al*., 2016b]. Previous work with thermal imagery of vegetation has focused predominantly on its application to agriculture and water management and availability [*Anderson et al*., 2012; *Gago et al*., 2015]. It has also been used previously to image tree temperatures in alpine forests to gain insight into the distribution of surface temperature of the canopy during snowmelt [*Ellis*, 2011; *Pomeroy et al*., 2009; *Webster et al*., 2016b]. So far, thermal imagery has largely allowed for simple visualization and interpretation of thermal structures in the forest at small spatial and temporal resolutions. Consequently, distributed measurements of canopy structure and surface temperature information would facilitate greater understanding of subcanopy incoming longwave radiation dynamics, providing insight to improve model estimations.

The purpose of this paper is to improve understanding of canopy temperatures and their influence on subcanopy incoming longwave radiation in heterogeneous forested environments and subsequently develop a simple parameterization for estimation of canopy temperatures within a distributed model that gives spatially explicit values. Canopy surface temperature data and measured subcanopy shortwave and longwave radiation were collected around a large gap and within a small gap in the adjacent forest across the 2015 and 2016 snowmelt seasons. Data collection and analysis focused on radiative regimes along the canopy edges in the four cardinal directions in the large gap and within the small gap. These locations broadly represent different canopy structure types relating to exposure to shortwave radiation: north edge (south facing,

exposed), east edge (west facing, exposed), south edge (north facing, exposed), west edge (east facing, exposed), and small gap (shaded, closed). Continuous meteorological and radiation measurements across the two snowmelt seasons were used to develop a simple parameterization for modeling subcanopy incoming longwave radiation based on a reference air temperature and subcanopy incoming shortwave radiation. This parameterization was then applied in a distributed model at 2 m point spacing across a heterogeneous forested area 170 × 220 m for an example clear-sky 24 h period.

2. Modeling Subcanopy Incoming Longwave Radiation

Total subcanopy incoming longwave radiation at a point is calculated by separation of the hemispherical view at a point into the sky (sky-view fraction, V_f) and canopy ($1 - V_f$) components:

$$\downarrow \mathrm{LWR}_{\mathrm{can}} = V_f \mathrm{LWR}_{\mathrm{ac}} + (1 - V_f)\left(\sigma T_{\mathrm{can}}^4\right) \quad (1)$$

where T_{can} is the temperature of the canopy, V_f is the sky-view fraction, and $\mathrm{LWR}_{\mathrm{ac}}$ is the measured incoming longwave radiation above the canopy. Because reflectance is not explicitly addressed in equation (1), an effective emissivity of 1 is assumed for the canopy [*Essery et al*., 2008].

Current methods used to obtain measurements of canopy surface temperatures are largely dependent on the use of thermocouples, both contact (TCs) and infrared (IRTCs), which obtain small-scale measurements. The limitation of these methods lies in the uncertainty of extrapolating single measurements across the entire canopy-view fraction ($1 - V_f$). For example, point measurements of tree trunk temperatures are often much higher than the surrounding canopy. Used as the representative canopy surface temperature within equation (1), a trunk temperature measurement would result in overestimations of subcanopy incoming longwave radiation, particularly during periods of high incoming shortwave radiation. Uncertainty therefore remains in extrapolating point measurements of canopy surface temperatures across larger areas of forests.

The continuing limitation of equation (1) is therefore the lack of information regarding the temperature of the canopy. Previous modeling efforts to estimate either canopy surface temperatures or subcanopy incoming longwave radiation have used parameterizations of above-canopy meteorological variables [*Essery et al*., 2008] or site-specific parameterizations of the relationship between shortwave radiation extinction and the canopy [*Pomeroy et al*., 2009]. These parameterizations are useful in that they relate canopy surface temperatures or longwave radiation to readily available above-canopy meteorological variables. However, a limitation remains in that the different parameterizations are either applicable to only a single point location in the subcanopy, or site-wide calibrated variables limit applicability to relatively continuous canopy structures. In particular, variables used in these methods mean that they are limited in application to relative closed-canopy environments where there is minimal direct exposure to shortwave radiative heating. Modeling in this study therefore focuses on the edges around a forest gap, where directional shortwave heating causes considerable variations in canopy surface temperatures and subsequently longwave radiation regimes between the four main cardinal directions: north (south exposed), east (west exposed), south (north exposed), and west (east exposed). Herein cardinal directions refer to the relative position in the clearing, not the direction of exposure. Canopy surface temperature measurements using IR imagery in these four locations in the gap were compared with those within a smaller gap, thus representing heterogeneity of the subcanopy environment in five functional classes.

3. Field Site Description

Data collection and modeling were carried out within a heterogeneous 170 × 220 m alpine forest site close to Davos Laret (46°50′42″N, 9°52′19″E, 1520 m above sea level) in eastern Switzerland (Figure 1). Measurements were conducted in a large angular gap approximately 70 × 50 m and a small gap within the adjacent forest approximately 20 × 10 m (Figure 1). Tree heights around the two gaps are between 12 and 35 m. Sky-view fractions at the center of the large and small gaps are 0.9 and 0.3, respectively. The study site was selected as it has minimal surface slopes and topographic shading. Tree species are predominantly Norwegian-spruce with some Larch trees, ranging from new growth up to 35 m in height. The corresponding open site was located approximately 250 m to the north-west of the clearing, used to represent above-canopy conditions. Data were collected throughout the snowmelt periods (March–April) in 2015 and 2016.

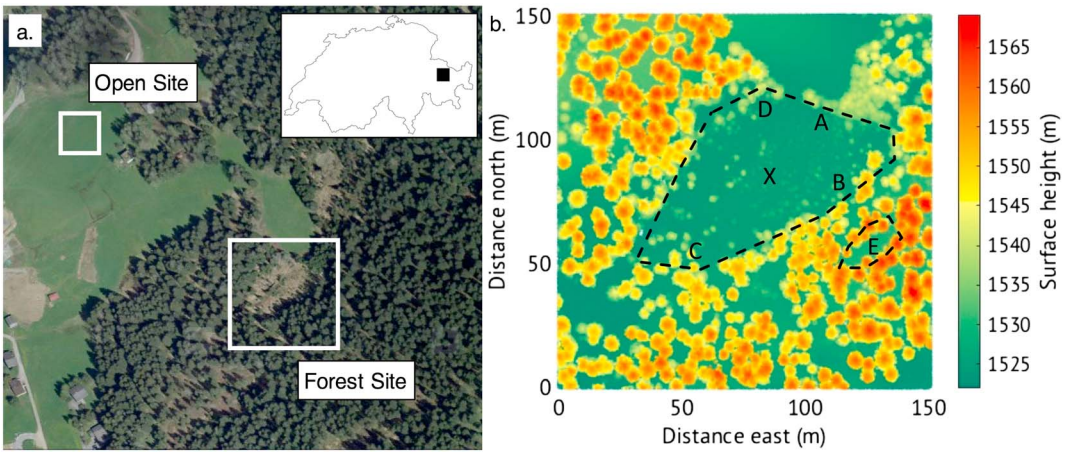

Figure 1. (a) Aerial photograph of Davos Laret showing location of reference open site and forest field site. (b) Overview of forest site from airborne lidar data. The dashed lines show outlines of the large gap and small gap within the forest. The lettering indicates locations of radiometer and temperature sensors at the north (A), east (B), south (C), and west (D) of the large gap and in the center of the small gap (E); The X denotes location in the center of the large gap where thermal images and reference air temperature measurements were taken; the color scale indicates surface/vegetation height from lidar data. Aerial photograph reproduced by permission of swisstopo (JA100118).

4. Data Collection and Processing

4.1. Radiation and Temperature Measurements

Incoming shortwave and longwave radiation were measured using 10 Kipp and Zonen CMP3 pyranometer and CGR3 pyrgeometer pairs. An open site comparison of these sensors during both clear-sky and cloudy conditions showed the pyranometers measured on average within 9 W m^{-2} and the pyrgeometers measured on average within 6 W m^{-2}. Radiometers were placed in distributed locations in and around the large and small gaps at Laret during springtime snowmelt (March–April) in 2015 and 2016. Data were thus collected at 20 different locations throughout the 2 years. Radiometers were placed at the north, south, and east edges of the large gap in 2015, and in 2016 radiometers were positioned at the west edge of the large gap and in the small gap (Figure 1b). A summary of the relative location and V_f values are shown in Tables 1 and 2. A single radiometer pair (Radiometer 6) was placed in the center of the large gap each year as a reference measurement. Radiometer locations were manually selected to best capture the different radiative regimes within the study area.

Each radiometer was placed on a rigid wooden platform, leveled and cleared of precipitation and interception daily. Periods of data where the radiometers were covered with snowfall, fallen interception, or were significantly tilted were removed during postprocessing. Data collected across the 2 years were used to calculate T_{eff} and validate modeled incoming longwave radiation in this study. Incoming longwave radiation was also measured at a nearby open site (Figure 1a) and taken to represent above canopy radiative conditions.

Table 1. Statistics for Radiometers in 2015 and Model Results Using Simply Air Temperature Within Equation (1) or the Corrections to Air Temperature in Equation (7) to Calculate T_{can} to Input Into Equation (1)[a]

			T_{air} Only		T_{air} Corrected	
Number	Canopy	V_f	Mean Bias	RMSE	Mean Bias	RMSE
1	N	0.43	6.7	7.65	2.68	4.11
2	N	0.41	10.74	10.85	3.42	6.23
3	G	0.81	8.48	8.71	6.8	7.07
4	E	0.44	7.97	8.6	4.1	4.97
5	C	0.21	9.95	10.37	3.69	4.65
6	G	0.91	2.73	3.39	1.49	2.8
7	S	0.49	13.06	13.06	9.25	9.3
8	S	0.34	10.54	10.7	5.73	6.18
9	C	0.36	12.38	12.39	7.04	7.21
10	C	0.41	10.39	10.41	5.11	5.54

[a]Model bias and RMSE are in W m^{-2}. Canopy environments are summarized as north (N), east (E), south (S), west (W), center of gap (G), and closed (C).

Air temperature was measured at 1 m above the snow surface using a thermistor housed in a naturally aspirated six-plate radiation shield. Measurement locations were established within 2 m of the radiometer pairs at the north, south, and east edges of the large gap in 2015 and

Table 2. As Table 1 But for Radiometers in 2016

			T_{air} Only		T_{air} Corrected	
Number	Canopy	V_f	Mean Bias	RMSE	Mean Bias	RMSE
1	C	0.27	10.52	11.51	5.51	7.71
2	C	0.27	8.34	9.03	3.95	6.07
3	C	0.19	4.9	6.66	−0.07	5.28
4*	C	0.24	4.66	6.39	−0.72	4.98
5	C	0.22	6.37	7.21	0.51	4.73
6	G	0.88	−1.03	5.57	−2.3	6.35
7	C	0.13	3.92	6.09	−2.81	6.16
8	C	0.25	8.06	8.55	2.59	4.58
9	W	0.52	7.79	9.31	2.35	7.65
10	W	0.52	4.54	6.62	−1.72	6.06

*Radiometer used for calibration of corrections in equations (5) and (6)

west edge of the large gap and within the small gap in 2016. Air temperature was also measured within the center of the large gap and was used as the reference air temperature for modeling incoming longwave radiation at all radiometer locations around the edges of the gap and within the small gap in the forest. The justification of this is that air temperature in the center of the gap is less influenced by the varied micrometeorology of the canopy and is more suitable for a site-wide reference air temperature similar to data often used to drive larger-scale snowmelt models. This location is herein referred to as the reference air temperature.

Continuous tree trunk temperatures were measured using pairs of Type-T contact thermocouples (TCs) consisting of copper and constantan conductors embedded just below the bark surface of the tree. During the 2015 snowmelt seasons thermocouples were installed in two trees (cf. Figure 3a) to capture reference tree trunk temperature measurements. Eight pairs were installed in tree 1 (west edge of large gap, sunny) between 1 and 1.8 m above the snow surface (these heights increased as the snowmelt progressed), and seven pairs were installed in tree 2 (east edge of large gap, shaded) at similar heights to those at tree 1. Pairs were located around the full 360° circumference of the trunk and were averaged to obtain one temperature value per tree trunk. Tree 1 was exposed to direct sunlight in the early morning and tree 2 received little direct sunlight but was in the area of the clearing that received sunlight shortly before sunset. All instruments were connected to Campbell CR1000 data loggers, measuring at 15 s intervals and averaging over 10 min periods.

4.2. Airborne Lidar Data

Lidar data of the study site were the same as that used within *Moeser et al.* [2014] and were used here to generate synthetic hemispherical photographs (HPs) for canopy classification and subsequent modeling on subcanopy incoming longwave radiation across the field site. Data were collected in September 2010 using a Riegl LMS Q560 sensor from multiple helicopter flyovers at a nominal flying altitude of 700 m for a total area of ~90 km^2. The wavelength emitted was 1550 nm, with pulse durations of 5 ns, and up to seven returns were detected per pulse for a maximum scan angle of ±15°. Postprocessing yielded an average echo density of 36 pulses per per square meter in the flyover domain and 19 pulses per square meter for the last returns (i.e., shot density) within the domain area. An affiliated digital terrain model was created by Toposys using their in-house processing software, TopPit (http://www.image-maps.com/toppit.htm), using the classified ground returns at a 0.5 m horizontal resolution.

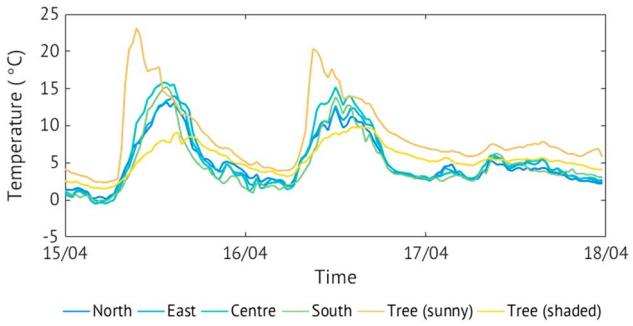

Figure 2. Measured air temperature in the north, east, south, and center of the large gap and tree trunk temperatures in the west and east of the large gap shown in Figure 1b throughout a 4 day period, including two clear-sky days (15–16 April) and two cloudy days (17–18 April) during the 2015 snowmelt season.

4.3. Canopy Classification

4.3.1. Optical Hemispherical Photographs (HPs)

Optical HPs were taken at each sensor location using a Canon 600D camera with a Sigma 4.5 mm F2.8 EX DC HSM fish-eye lens mounted on a metal plate that allowed easy leveling and orientation of the lens. Manual thresholding was used to characterize the pixels into either black (canopy) or

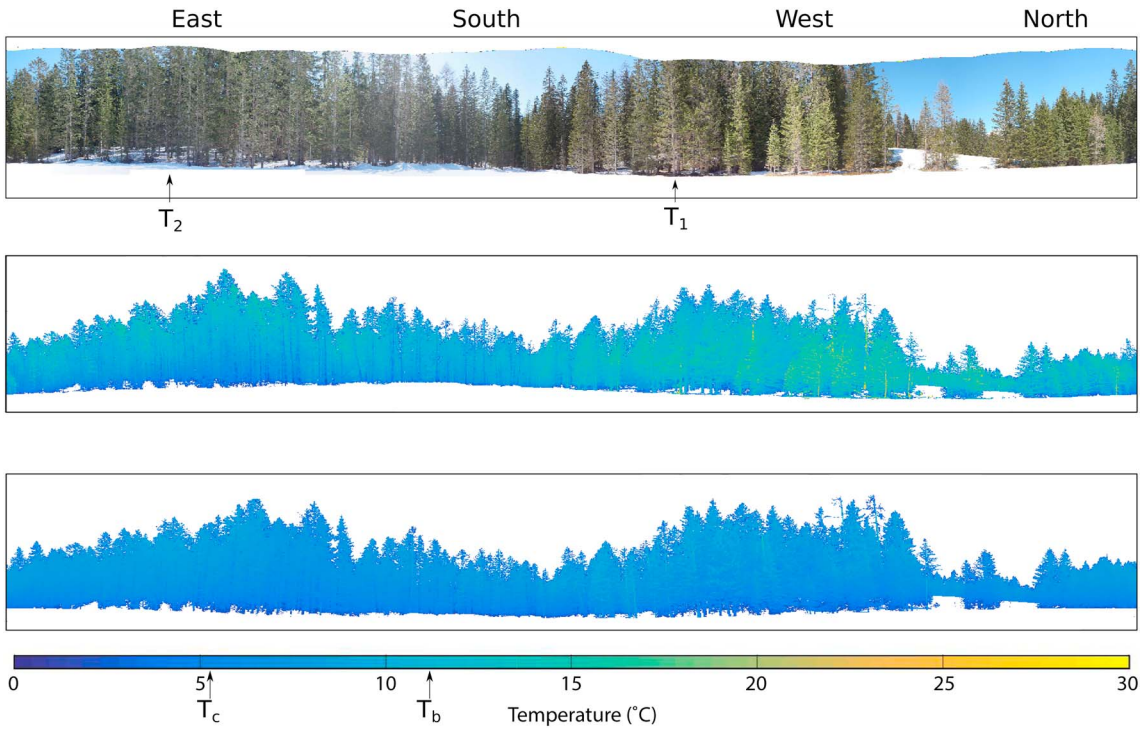

Figure 3. (a) Optical image of 360° canopy edge around the large gap and associated thermal images on (b) a clear-sky day 20 April 2016 at 13:00 and (c) a cloudy day 30 March 2016 at 10:00. T_1 and T_2 indicate positions of trees installed with thermocouples (Tree 1 and Tree 2, respectively). T_b and T_b indicate reference air temperature during imaging of thermal images in Figures 3a and 3b.

white (sky) pixels [*Reid and Essery*, 2013]. V_f was calculated from the ratio between the numbers of canopy and sky pixels in each concentric ring weighted by the sine of the elevation angle according to *Essery et al.* [2008]. Values of V_f used for calculation of T_{eff} and validation of equation (1) were calculated from the optical HPs taken at the exact location of each radiometer to ensure maximum accuracy.

4.3.2. Synthetic Hemispherical Photographs

In order to incorporate an angular viewpoint for generating synthetic HPs, the lidar data were converted into a spherical coordinate system following *Moeser et al.* [2014]. Using these methods, *Moeser et al.* [2014] demonstrated the similarities of synthetic and optical images in calculating canopy closure (closely related to V_f) and LAI′. The advantage of synthetic HPs over manual optical images is that the method makes V_f attainable for hundreds of locations within the subcanopy throughout the field area at Laret.

Synthetic HPs can be generated at any location within the lidar point cloud by specifying the location (the origin). Cartesian coordinates (*xyz*) were converted into three variables: the elevation angle (θ), the angle between the positive *x* axis and the projection point on the *x*/*y* plane (ϕ), and the distance from the origin to the point (*r*). For each point, θ was calculated from 0–90° and ϕ flipped east-west for a full 180° view frame. The θ values were then flipped on the east-west axis to mimic the upward viewing projection of HPs.

Calculation of V_f from the synthetic HPs followed the same weighting procedure applied to the optical HPs. Thresholding of the images was not required for synthetic HPs as they were already created in binary format.

4.4. Thermal Imaging

Thermal images presented in this study were taken during the snowmelt period in 2016 using a VarioCAM® high-resolution inspect 768 (RE) Jenoptik thermal camera with an infrared image resolution of 1024 × 768 pixels that operates at 7.5 to 14 μm and has an accuracy of ±1.5% (K). Emissivity was set to 1 for all imaging scenarios. The camera was factory calibrated by the manufacturers when purchased in 2013.

Complete panoramic images of the surface edge of the large and small gaps were captured during the 2016 snowmelt period. The camera was set on a leveled tripod at approximately 50 cm above ground in the center

of the large gap and was handheld in the center of the small gap due to angular constraints of the tripod. The size of the small gap and the shape of the canopy required pointing the thermal camera up at the canopy, mimicking the view from the radiometer.

Days for thermal imaging were selected based on several different criteria. Imaging took place on days when there was no intercepted snow on the canopy, as that would bias infrared estimations of canopy surface temperature, or when no precipitation was falling due to its influence on radiometer measurements. Imaging days were also selected to cover a range of meteorological conditions including days of clear sky or a mixture of cloudy and sunny.

Different surfaces in the thermal images have different emissivities. Reflectance of energy is assumed to be negligible and so the emissivity of the canopy was assumed to be 1. Due to the 3-D nature of the canopy, particularly the cylindrical tree trunks, emissivity will vary with viewing angle [*Sobrino and Cuenca*, 1999]. These effects are most noticeable around the edges of tree trunks; however, the resolution of the camera used in this study and the distance from the camera to the canopy edge means that these small-scale differences in measured surface temperatures are negligible. Snow and sky captured in the images have varying values of effective emissivity, depending on cloudiness and water vapor (sky [*Liston and Elder*, 2006]) and viewing angle (snow; *Dozier and Warren*, 1982]); however, as these were not the focus on the thermal images, the differences in emissivity of snow and sky were ignored.

Snow and sky pixels had an effective temperature below 0°C in all thermal images, while tree temperatures measured at the two TC trees were above 0°C during all imaging periods. Using this information, any pixels in the raw images below 0°C were assumed to represent sky or snow and were subsequently removed from the analysis files. Despite this filtering, mixed pixels that integrate canopy and sky temperatures remained in the images if they were above 0°C, thus reducing the accuracy of the data around the top edges of the canopy. Further effects on image accuracy arising from surface roughness and air temperature/humidity were deemed to be negligible due to the proximity of the canopy to the camera ($<$ 50 m); atmospheric effects tend only to cause accuracy issues at distances greater than 100 m [*Ball and Pinkerton*, 2006].

4.5. Determination of Forest Temperatures From Thermal Images

Raw IR temperature files were converted to gray scale images using MATLAB R2015 software (Mathworks Inc.). Individual images were then stitched to a single composite image using Microsoft Image Composite Editor (Microsoft Research) to allow evaluation of spatial distributions of canopy surface temperatures around the edges of both gaps.

The difference in viewing angles from the camera positions at the two locations created two different panoramic views (cf. Figures 4a and 5a). The distance from the camera to the canopy in the large gap created a full view of the height of the canopy, including the tops of the trees. The proximity and angle of the canopy relative to the imaging location within the small gap meant that the camera was looking up at the top of the canopy, similar to the hemispherical view from a radiometer, resulting in a Mercator-like projection in the panoramic image. It is also likely that the top of the canopy was obscured in the thermal panoramic images of the small gap.

Following stitching, gray scale images were back-calculated to individual pixel temperature following the methods in *Cohen et al*. [2005]. The temperature of each pixel was calculated from the 8 bit gray level image using:

$$T_{(x,y)} = \left(\mathrm{GL}_{(x,y)}.T_{range}\right) - T_{min} \tag{2}$$

where $T_{(x,y)}$ is the calculated temperature at each pixel (x,y), $\mathrm{GL}_{(x,y)}$ is the gray level of pixel (x,y) in the 8 bit image, T_{range} is the difference between maximum and minimum temperature in the image, and T_{min} is the minimum temperature, both of which were predetermined from the raw data files.

Because distance to the canopy was different in each direction, a "relative height" descriptor (h/z_d) was used to represent canopy height in the thermal images instead of absolute height measurements from the lidar data. Relative height describes the fraction of forest height (h) relative to the total vertical depth of the canopy (z_d), varying along the horizontal canopy profile. The relative height was determined by manually selecting the canopy top and bottom along the entire canopy gap edge in each IR image. The result is expressed as a percentage, where 0% corresponds to the snow surface and 100% corresponds to the

highest point in the canopy. The top of the canopy (100% relative height) therefore changes in absolute height (m) along the 360° panoramic around both the small and large gaps.

Segments of each panoramic image were subset in order to further investigate differences in canopy surface temperature in the different cardinal directions. Around the large gap, thermal images were separated based on the corresponding view fraction of the radiometers placed in each of the four locations. The maximum height in each of the four segments was used as the canopy top for relative height calculation. Within the small gap, the image was divided into four even segments based on cardinal direction. Due to the fairly uniform relative height in the small gap, the same top of canopy location was used for each of the four segments.

4.6. Determination of Forest Temperatures From Radiation Measurements

Canopy temperature measurements were also obtained through the calculation of effective emitting temperature of the canopy (T_{eff}). T_{eff} was calculated using measured incoming longwave radiation ($\mathrm{LWR}_{\mathrm{meas}}$) from the radiometers in the subcanopy and inverting equation (1):

$$T_{eff} = \left(\frac{\mathrm{LWR}_{meas} - (V_f \mathrm{LWR}_{ac})}{(1 - V_f)\sigma\varepsilon_{can}}\right)^{0.25} - 273.15 \tag{3}$$

to obtain T_{eff} in °C.

4.7. Model Improvements

A new parameterization for predicting canopy surface temperatures was developed using subcanopy shortwave radiation as a predictor variable. Subcanopy shortwave radiation was used as it better represents penetration of shortwave radiation and subsequent heating of the canopy. This creates spatially variable canopy surface temperatures compared to using above-canopy measurements, which result in a single site-wide value. A multiple linear regression model was therefore developed following:

$$T_{can} = \beta_0 + \beta_1 . \downarrow SWR_{sc} + \beta_2 . T_{air} \tag{4}$$

where $\downarrow \mathrm{SWR}_{\mathrm{sc}}$ is measured (or modeled) subcanopy shortwave radiation (W m^{-2}) and β_0, β_1, and β_2 are calibrated regression coefficients. A simple multiple linear regression was chosen due to its proven effectiveness in prediction of canopy surface temperature or longwave radiation in previous studies [*Essery et al*., 2008; *Howard and Stull*, 2013].

Further modeling at a distributed scale was carried out using the lidar data and calculation of V_f from synthetic hemispherical photographs (HPs) at 9632 locations at 2 m grid spacing in the 170 × 220m field area (Figure 1b). Estimates of subcanopy longwave radiation at 10 min intervals used canopy temperatures calculated using equation (4) on 12.04.2016 (clear-sky day). Subcanopy incoming shortwave radiation was estimated using synthetic HPs and the algorithms in the software *Hemisfer* [http://www.wsl.ch/dienstleistungen/produkte/software/hemisfer/, *Thimonier et al*., 2010] following the methods in *Moeser et al*. [2014]. These calculated values were then used to estimate subcanopy longwave radiation throughout the 24 h period.

5. Results

5.1. Canopy and Air Temperature Variations

Figure 2 demonstrates spatial and temporal variations in measured air and tree trunk temperatures on either side of the large gap on both clear-sky (15–16 April) and cloudy (17–18 April) days during the 2015 measurement period. Air temperatures were measured at four different locations; in the north and south the temperature measurements were located below the canopy, whereas in the center and in the east the measurements were located away from the canopy. During the two clear-sky days, air temperatures at all locations were close to 0°C at night and increased to between 10 and 13°C during the day. Temperature differences between the four locations varied by no more than 4°C, with air temperature highest in the center of the clearing compared to the north and east edges of the gap, although nighttime temperatures were warmest in the north and south locations, where the air temperature thermistors were within in the subcanopy. Comparatively, during the two cloudy days, measured air temperature in the gap and in the subcanopy showed a spatial variation less than 2°C.

Daily variations and differences between tree trunk temperatures on opposite sides of the large gap were greater than those seen in measured air temperature (Figure 2). Temperatures of individual thermocouple

pairs varied by a maximum of 5°C around the tree in the east (shaded) and 14°C around the sunny tree in the west. The two trees maintained temperatures above measured air temperatures during both nighttime periods and cloudy days. The tree in the west of the large gap increased to temperatures above 20°C following sunrise and gradually declined in temperature throughout the day. In contrast, average temperature of the shaded tree in the east remained below all four measurements of air temperature from 08:00 until 18:00, and daily variation was below 10°C.

Differences between canopy surface temperatures around the gap on clear-sky and cloudy days are also demonstrated in the two thermal images of the edge of the large gap in Figure 3. Sun-lit north and west edges, exposed to direct solar heating under the clear-sky conditions, were, on average, up to 10°C warmer than the canopy along the shaded south and east edges. Surface canopy temperatures were also warmer than measured reference air temperature in the center of the gap (T_{air} = 12°C) at the time of imaging. During the cloudy day (Figure 3c), the canopy was relatively uniform in temperature in comparison to the clear-sky day, and overall was slightly warmer than reference air temperature (T_{air} = 5°C).

Tree trunks in particular showed different surface temperature variations between the clear-sky and cloudy days. During the cloudy day, tree trunks showed small (<4°C) differences relative to the surface temperature of the surrounding canopy, and differences in tree trunk surface temperatures between the Sun-lit and shaded sides of the gap were <5°C. In contrast, during the clear-sky day, tree trunks showed much greater variations in surface temperatures. Along the Sun-lit edges of the gap, tree trunk surface temperatures were as high as 30°C, 18°C warmer than the temperatures of the surrounding canopy. Additionally, larch tree trunks reached temperatures up to 30°C, while spruce tree trunks were closer to 20°C. Along the shaded edges, tree trunk surface temperatures were closer to 5°C, lower than the surfaces temperature of the surrounding canopy. These spatial differences resulting from direct solar heating of the tree trunks were also shown in the contact tree trunk temperature measurements in Figure 2. It is likely that the substantial increases in tree trunk surface temperatures in these regions around gaps are the main contributor to subcanopy incoming longwave maxima along Sun-lit gap edges.

Vertical variations in canopy surface temperatures all around the four edges of the large gap were apparent in the IR image taken during clear-sky conditions (Figure 3b). At the north and west edges of the gap, the top of the canopy (above 90% relative height) can be seen to be cooler than the canopy below. It is possible that this negative temperature profile is from a combination of evaporative and convective fluxes from wind shear at the top of the canopy, a greater thermal mass of the lower canopy, or a result of mixed-pixels in the thermal images—averaging temperature over pixels that contain both sky and canopy in the images. Along the shaded edges (south and east) the upper 20% (relative height) of the vertical profile of the canopy can be seen to be warmer than the lower canopy, where it is exposed to more incoming shortwave radiation from behind. In comparison, limited vertical variations in canopy temperatures were visible in the thermal image taken on the cloudy day, suggesting that spatial variations in canopy surface temperatures around discontinuities do not need to be incorporated in subcanopy incoming longwave radiation models during cloudy periods, as the canopy exhibits a relatively uniform surface temperature close to measured reference air temperature. However, spatial variability in canopy surface temperatures during clear-sky conditions requires further attention for modeling applications.

Differences in horizontal and vertical variability in canopy surface temperatures during clear-sky conditions are shown for both the large gap (Figure 4) and small gap (Figure 5). Canopy surface temperatures along the horizontal profile at 30% relative height show temperatures below air temperature at the shaded south and east edges of the large gap. Sun-lit edges of the gap show an elevation of canopy surface temperatures above reference air temperature in the center of the gap up to 18°C. Peaks up to 28°C along the horizontal profile represent solar heated tree trunks, reflecting the point measurements of tree trunk temperature at the west edge of the gap (Figure 2).

Within the small gap, horizontal variations at 30% relative height exhibited relatively little change around the gap edge compared to that seen around the large gap (Figure 5b). Canopy surface temperatures were approximately 1–2°C warmer than reference air temperature in the west and north, and closer to reference air temperature in the south and east. Periodic decreases in surface temperature along the horizontal profile indicate that tree trunks were cooler than the surface temperature of the surrounding canopy by up to 5°C. These cold tree trunks again match measurements of the individual tree trunk temperatures at the east edge

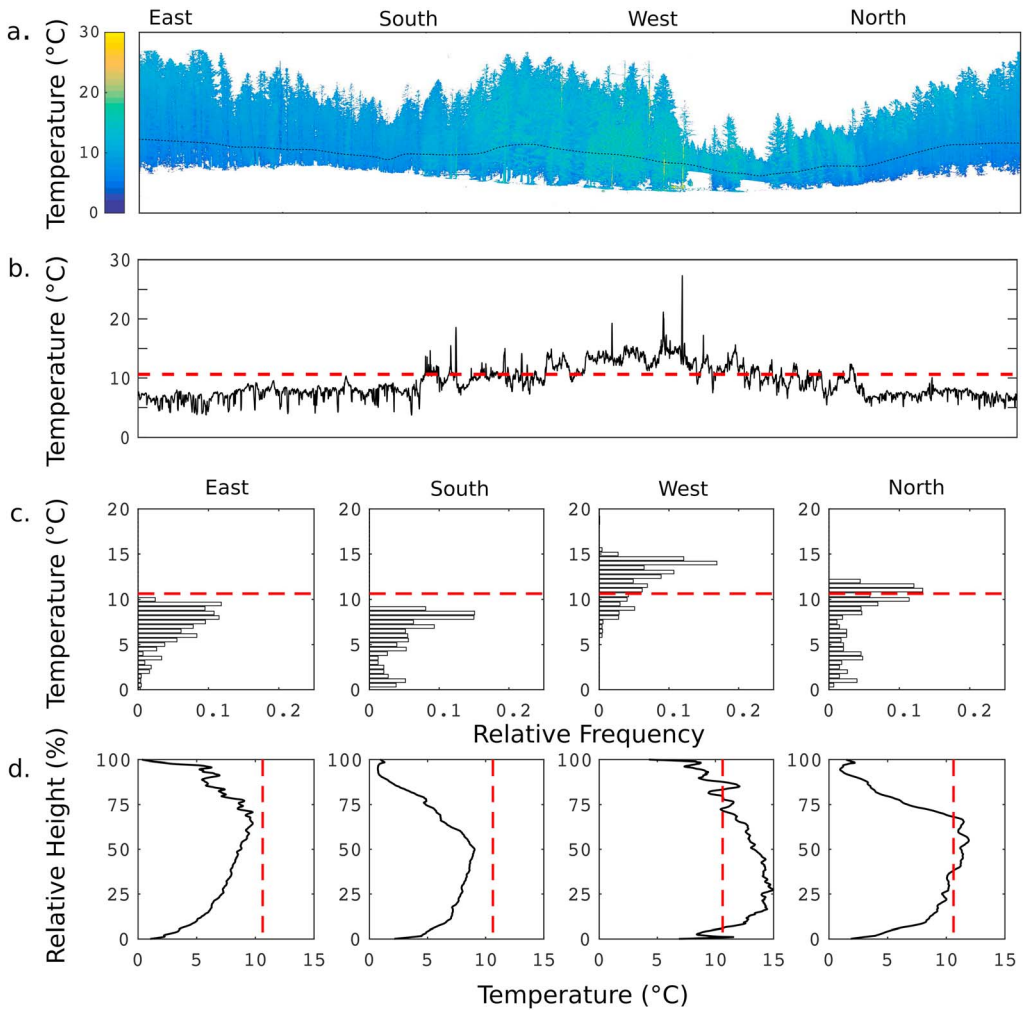

Figure 4. (a) Spatial variations in canopy surface temperature in the large gap at 12:00, 20 April 2016, (b) horizontal temperature distribution at 30% relative height (black line in a), (c) relative frequency distribution of canopy temperature in the vertical profiles at the four cardinal directions around the gap, (d) vertical temperature profiles with relative canopy height (dimensionless) in the four cardinal directions around the gap. The red dashed lines indicate air temperature measured in the middle of the large gap at time of imaging.

(shaded) of the large gap (Figure 2), where trunk temperatures were also colder than reference air temperature during clear-sky conditions.

Relative frequency temperature distributions of the vertical profiles at the four edge locations around the large and small gaps further demonstrate the spatial variations in canopy surface temperatures (Figures 4c and 5c). Peaks in the distributions of temperature throughout the vertical profiles at the north and west edges were between 13 and 16°C, whereas peaks in the distributions at the east and south edges were below air temperature. Directional frequency distributions in the small gap showed less variation than in the large gap. Peaks in the distributions at the north and west edges were close to 15°C, whereas peaks in the distributions at the south and east aspects were again below air temperature.

Vertical temperature profiles at the four edges were greater in the large gap than within the small gap (Figures 4d and 5d). In the large gap, vertical temperature profiles increased above air temperature at the sunny west and north edges of the large gap but were below air temperature in the east and south. In the west, exposed to direct sunlight, most of the vertical profile was at or above air temperature, particularly between 10 and 80% relative height. Vertical gradients at the other three locations were cooler in the lower canopy, between 5 and 8°C below air temperature, and increasing up to 2°C below air temperature in the south and east and 1°C above air temperature in the north. At all four locations, canopy surface

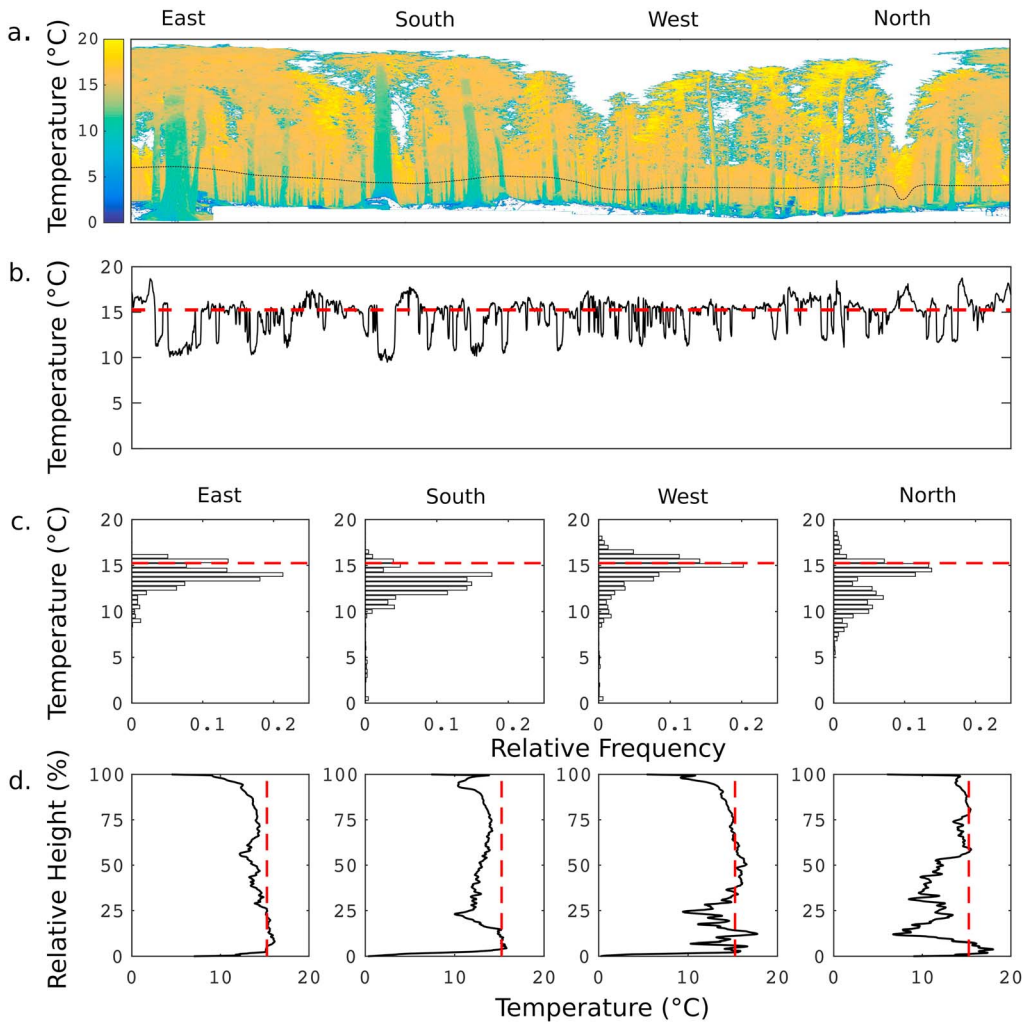

Figure 5. As Figure 4 but within the small gap at 12:00 21 April 2016.

temperatures decreased above 70% relative height, although this decrease was less pronounced at the Sun-exposed west edge.

Vertical temperature profiles showed more uniform variation at the four edges around the small gap compared to the large gap (Figure 5d). With the exception of a cold patch in the profile on the north side of the small gap, all four vertical profiles were within 2–3°C of air temperature. This lack of directional variability shown in canopy surface temperatures in Figure 5 suggests that the direction of exposure of the canopy has minimal effect within shaded canopies, away from forest edges exposed to direct incoming shortwave radiation.

5.2. Modeling Incoming Longwave Radiation

Thermal images of the canopy within the small gap suggest that the canopy surface is close to or below air temperature during daytime clear-sky periods (Figure 5). This was further assessed across a 24 h clear-sky period through the calculation of effective emitting temperature of the canopy (T_{eff}) using equation (3). The results of this calculation over a 24 h clear-sky period are shown in Figure 6a for radiometer 5 in 2016. Daytime reference T_{air} and T_{eff} were relatively similar (within 1°C) and followed the same temporal trend of increasing in the morning following sunrise and decreasing in the afternoon and evening following solar noon. Before sunrise and after sunset, reference air temperature was approximately 3°C below T_{eff}, suggesting that at night, canopy temperatures within denser environments remain warmer than T_{air}. This was also shown in the point thermocouple measurements in Figure 2.

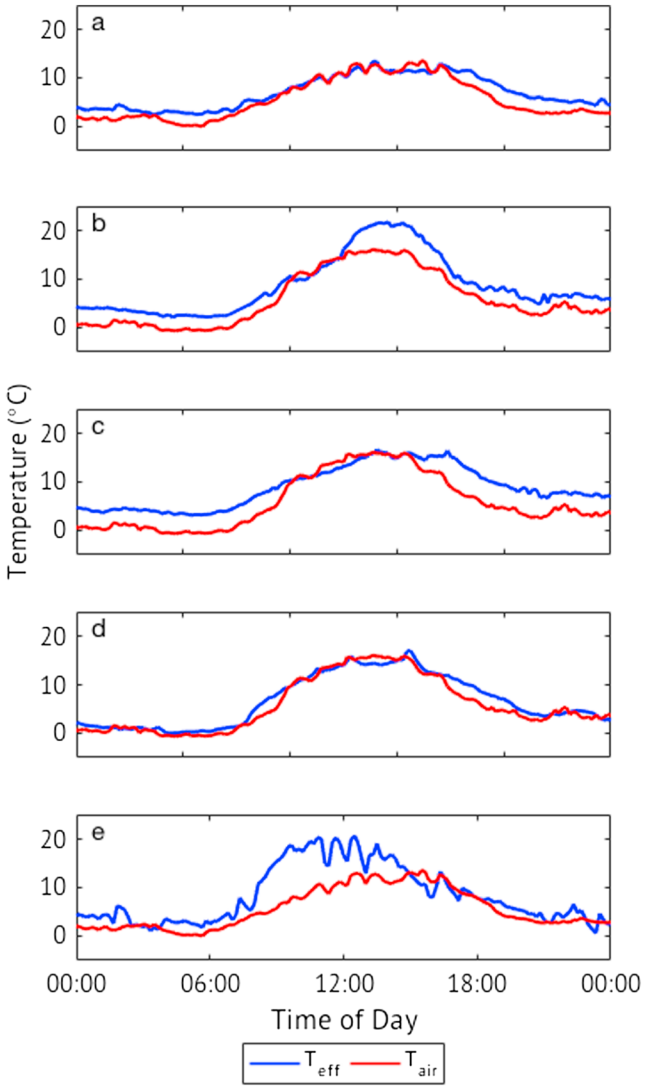

Figure 6. Time series showing calculated T_{eff} and measured reference air temperature across a (a) clear-sky 24 h period in the small gap (radiometer 5, 2016), (b) north edge of the large gap (radiometer 2, 2015), (c) east (radiometer 4, 2015), (d) south (radiometer 8, 2015), and (e) west (radiometer 10, 2016) on 15 April 2015 (Figures 6b–6d) and 12 April 2016 (Figures 6a and 6e).

Differences between T_{air} and T_{eff} within the small gap during the snowmelt period are further demonstrated in the performance of using measured reference T_{air} in equation (1) at the radiometer locations in closed environments throughout the 2015–2016 snowmelt seasons (March–April) (Tables 1 and 2). Underestimations by the model were largest particularly when incoming longwave radiation was low (<320 W m^{-2}), likely during nighttime conditions when the canopy remains warmer than reference T_{air} in the center of the gap. These estimates of incoming longwave radiation using air temperature suggest that errors throughout a snowmelt season are not compensated, and continuous underestimation throughout nighttime periods would overall reduce the total amount of melt energy in these locations, delaying modeled snow disappearance date.

Offset of the canopy to the reference air temperature is approximately 3°C throughout the times in the 24 h period when subcanopy shortwave radiation was 0 W m^{-2}, suggesting that a simple correction to measured air temperature can be applied during these periods:

$$T_{can} = T_{air} + x \quad (5)$$

where x is the site-calibrated bulk offset applied to measured reference air temperature to reduce model bias. This suggests a simple method for estimating T_{can} from T_{air} in small gaps, which are representative of closed canopy environments with minimal direct subcanopy shortwave heating. A local bulk offset could be calibrated conditionally on radiometer data being available to calculate a value representative of a site or region. However, the relatively low root-mean-square error (RMSE) of the simple air temperature model at most radiometer locations, particularly in the shaded sides of gap and within the closed environments with low V_f values (Tables 1 and 2), indicates that a reference air temperature (i.e., a zero offset) can be a suitable predictor of canopy temperature for modeling subcanopy incoming longwave radiation.

Calculated T_{eff} from the pyrgeometers placed at the four edge locations around the large gap showed different thermal regimes compared to that seen in the small gap (Figures 6b–6e). The time series of T_{eff} across a 24 h clear-sky period illustrates heating of the canopy above T_{air} during daily increases in shortwave radiation, particularly at the west, north, and east edges. T_{eff} increased above air temperature in the morning (west), during midday to afternoon (north), and in the evening (east), reflecting the movement of the daily solar track. The southern side of the gap (i.e., never exposed to direct shortwave radiation) maintained T_{eff} close to measured reference air temperature throughout the entire 24 h period. These increases in canopy surface temperature reflect the movement of the daily solar track and are not represented in subcanopy incoming

longwave radiation models relying solely on air temperature. There were periods of the day, particularly in late morning and early afternoon, when calculated T_{eff} in the south and east edges were lower than measured air temperature by 2–3°C, likely caused by minimal shortwave heating in the shaded areas compared to the center of the large gap.

Differences in canopy temperatures at the four locations in the large gap were also apparent at nighttime. T_{eff} in the west, north, and east remained above or close to air temperature, whereas the canopy in the south had an effective temperature very close to air temperature. These differences can be explained by the locations of the individual radiometers. The radiometer in the south was placed in an area of smaller trees with an indistinct gap edge compared to the other three locations around the gap where the radiometers were located at a distinct canopy edge. These temperature variations were different to those seen in the smaller gap, where T_{eff} during nighttime remained higher than T_{air}, suggesting a greater loss of energy from the canopy to the atmosphere in the large gap that was attenuated in closed canopy environments.

Elevations in calculated T_{eff} above reference air temperature along the edges of the large gap indicate a need for correcting for exposure of the canopy to shortwave radiation when estimating subcanopy incoming longwave radiation. A new parameterization for predicting canopy surface temperature was developed using measured subcanopy shortwave radiation as a predictor variable as it better represents the spatial and temporal variations in direct canopy heating compared to above-canopy measurements. Calibration data were the same as that used to calculate the bulk offset in equation (5). Measurements of reference air temperature and subcanopy shortwave radiation from a single radiometer location within the subcanopy across a single clear-sky 24 h period (12 April 2016) were combined to develop a multiple linear regression model (equation (4)) using T_{air} and subcanopy incoming shortwave radiation as predictor variables:

$$T_{can} = 2.36 + 0.88T_{air} + 0.0073{\downarrow}SWR_{sc} \tag{6}$$

where $\downarrow SWR_{sc}$ is measured subcanopy incoming shortwave radiation and T_{air} is in °C to give T_{can} in °C. Model RMSE was 0.7°C with an adjusted R^2 of 0.93 across the 24 h calibration period. All coefficients were statistically significant at the 99% confidence level.

Equations (5) and (6) were then combined to predict subcanopy incoming longwave radiation at all 10 radiometer sites throughout the 2015 and 2016 snowmelt seasons, at a total of 20 different locations. The correction to T_{can} in equation (5) was applied only at nighttime, when measured subcanopy shortwave radiation was 0 W m^{-2}. Additionally, the correction for subcanopy shortwave radiation was only applied when measured values exceeded 400 W m^{-2}. This value was chosen to be representative of locations exposed to direct shortwave radiation along gap edges. Analysis of measured data found that subcanopy shortwave radiation does not exceed this value in the relatively closed canopy environments where air temperature suitably represents canopy temperatures during daytime periods. The corrections to T_{air} were applied as follows:

$$T_{can} = \begin{cases} SW_{sc} = 0, & T_{air} + x \\ 1 \leq SW_{sc} \leq 400, & T_{air} \\ SW_{sc} > 400, & \beta_0 + \beta_1 T_{air} + \beta_2 SW_{sc} \end{cases} \tag{7}$$

for input of T_{can} into equation (1).

Results of subcanopy incoming longwave radiation estimated at all 20 radiometer locations throughout the 2015 and 2016 snowmelt seasons (March–April) are summarized in Tables 1 and 2. Using the three T_{air} parameterizations for input of T_{can} into equation (1), seasonal model RMSE and mean bias of estimated subcanopy incoming longwave radiation were reduced at all but two radiometer locations compared to using T_{air} alone. RMSE remained within 1 W m^{-2} at radiometers 6 and 7 in 2016. Maximum decrease in mean bias was by 7.3 W m^{-2} at the radiometer on the north side of the gap in 2015 (Figure 7a), and smallest decreases in mean bias were at the radiometer located in the center of the clearing (radiometer 6 in 2015 and 2016). While the maximum decrease in seasonal average mean bias was 7.3 W m^{-2}, reductions were largest during time periods when multiple linear regression was applied. Outside these time periods, either air temperature or the bulk offset was used. At the same radiometer at the north side of the gap (Figure 7a), model RMSE was reduced from 20.1 to 6.6 W m^{-2} when the multiple linear regression correction was required. Maximum reductions in model bias at individual time steps were also up to 30 W m^{-2} in Sun-lit locations.

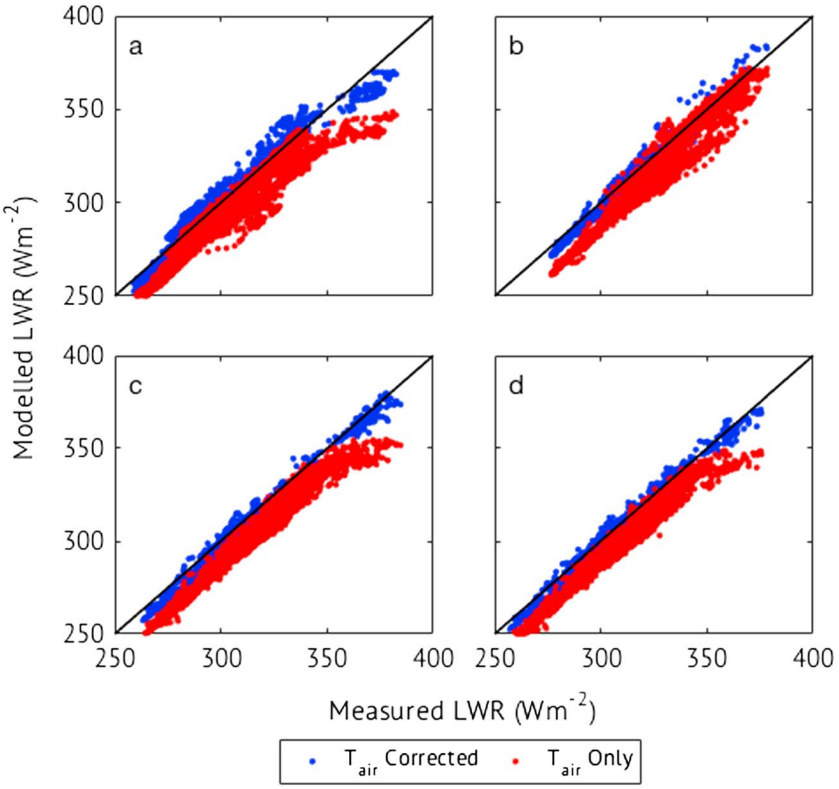

Figure 7. Measured and modeled subcanopy incoming longwave radiation during the 2015 snowmelt season (March/April) using either only air temperature to represent canopy temperature (T_{air} only) or the correction parameterizations in equation (7) to estimate T_{can} (T_{air} corrected) at radiometers (a) 2, (b) 5, (c) 9, and (d) 10.

Modeled subcanopy incoming longwave radiation using either T_{air} or the correction parameterizations are shown in Figure 7 for the four radiometers that showed the greatest reduction in RMSE using the correction parameterization. The largest underestimations of the T_{air}-only model occurred during periods of high subcanopy incoming longwave radiation, coinciding with elevated canopy heating by shortwave radiation. During these periods, errors were substantially reduced through the introduction of equation (6), especially at radiometers 2, 9, and 10 in 2015 (Figures 7a, 7c, and 7d). Reductions in RMSE during periods of subcanopy shortwave radiation greater than 400 W m^{-2} at radiometers 9 and 10 were 22.1 to 3.3 W m^{-2} and 18.7 to 3.4 W m^{-2}, respectively. Additionally, during periods of low subcanopy incoming longwave radiation, the nighttime bulk offset approach reduced the underestimations of the T_{air} only model at all four locations shown in Figure 7.

The correction parameterizations in equation (7) were then applied at 9632 locations in the 170 × 220 m field area using modeled potential incoming solar radiation. The results are compared to the simple air temperature model in Figure 8 at three hourly periods from 9 A.M. to 6 P.M. These corrections for canopy temperature better represented canopy exposure to solar radiation as well as shading by the canopy. Exposure to solar radiation was particularly apparent in the increases in longwave radiation along the Sun-exposed edges of the gap relative to the Sun position between 09:00 and 15:00. For example, at 12:00 there was minimal radiation along the south-east edge of the gap, reflecting the shape of the canopy and relative shading, compared to increased radiation on the north side of the gap. Additionally, in the discontinuous areas in the surrounding forest (see tree locations and forest structure in Figure 1b) the new model allowed for representation of increased heating of the canopy surface by shortwave radiation due to the heterogeneous nature of the canopy structure. These variations were not represented in the air temperature model, which did not resolve for the small-scale variability in incoming longwave radiation, which decreased with increasing distance to the canopy as a function solely due to variations in sky-view fraction.

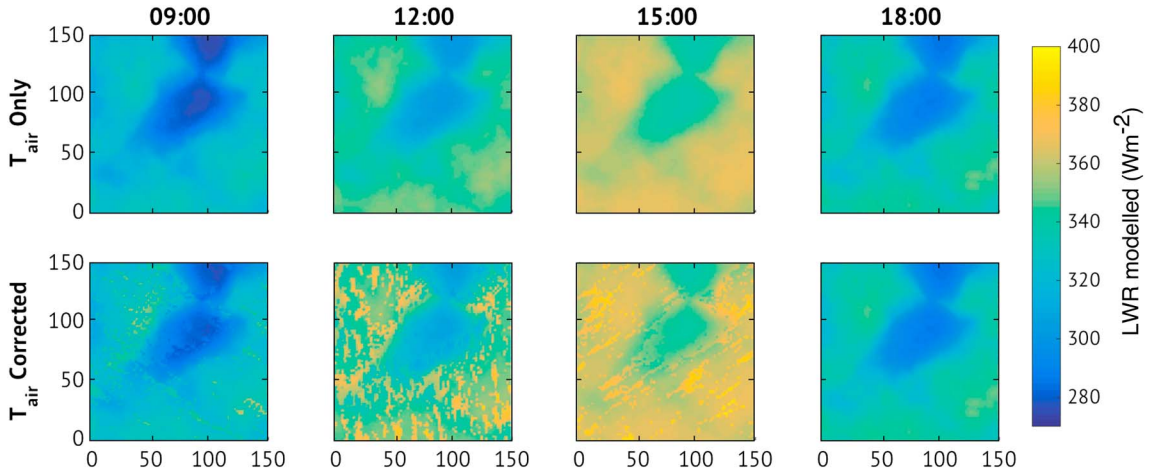

Figure 8. Modeled subcanopy incoming longwave radiation at 2 m grid spacing over the field site area (Figure 1b) using (top) only reference air temperature or the (bottom) correction parameterizations in equation (7) on 12 April 2016. Results shown are for 09:00, 12:00, 15:00, and 18:00. The values of *x* and *y* axes are in meters.

6. Discussion

Spatial variation in measurements of air temperature around a large canopy gap have important implications for canopy temperature calculations. Results showed that nighttime canopy surface temperatures were warmer than the reference air temperature in the center of the large gap; however, air temperatures within the subcanopy would likely be more representative of canopy temperature measurements. The selection of air temperature for estimating canopy surface temperatures is clearly an important step in subcanopy longwave radiation modeling. While a local subcanopy air temperature measurement is most likely the best representative value for calculating longwave radiation, these air temperatures have been shown here to vary both spatially and temporally. A single subcanopy air temperature is likely not suitable for an entire heterogeneous subcanopy environment, like the one investigated in this study. Additionally, unless a study is a specialized subcanopy energy balance or snowmelt study, subcanopy measurements of air temperatures are not readily available, and it is even more uncommon for these measurements to be available continually across interseasonal time scales to drive multiyear operational snowmelt models.

Thermal images of canopy surface temperatures around the large and small gaps demonstrate pronounced spatial and temporal variations. Canopy surface temperatures measured using IR imagery in both gaps varied up to 18°C above reference air temperature. Measured canopy surface temperatures in the shaded edges and small gap were up to 20°C lower compared to temperatures measured at the Sun-lit edges of the large gap during clear-sky conditions. These temperature differences further demonstrate the significance of canopy discontinuities, where gaps act as radiative "hot spots" due to co-located shortwave and longwave radiation maxima at the north forest edge [*Lawler and Link*, 2011; *Seyednasrollah and Kumar*, 2014].

During cloudy periods, spatial variation of canopy surface temperatures was low due to the lack of direct canopy heating from shortwave radiation. In particular, canopy surface temperatures around the large gap remained within 3°C of reference air temperature measured in the center of the large gap, and differences between trunk and needle/branch temperatures were within 1°C. Spatial variations around the small gap, including during clear-sky periods, were within 1–5°C. A lack of directional difference in measured canopy surface temperatures supports the theoretical findings in *Seyednasrollah and Kumar* [2014], who showed relatively small spatial gradients in subcanopy incoming longwave radiation in gaps with diameters less than half of the surrounding tree height, i.e., similar size to the small gap investigated in this study. With limited subcanopy heating by shortwave radiation in these environments, reference air temperature was close enough to canopy temperature measurements to be used in estimating subcanopy longwave radiation without the need for corrections or offsets, coincident with the conclusions by *Sicart et al*. [2004].

Differences of 1–3°C between canopy temperatures and measured reference air temperature were seen both during cloudy conditions, particularly within the small gap, but also along the edges of the larger gap. Measured temperatures therefore suggest that during day-time cloudy periods, air temperature can be

used within equation (1), without a correction required for incoming shortwave radiation and subsequent canopy heating. Similar conclusions have been made in the field-based study by *Pomeroy et al*. [2009], who used point measurements of canopy temperatures to demonstrate that air temperature can be a good estimate of canopy temperature under low insolation conditions.

While air temperature can be a good substitute for canopy temperature during cloudy conditions in sparse canopies and in closed canopy environments under all-sky conditions, a further improvement was made through the use of a bulk offset method applied at nighttime. The requirement of a nighttime offset in this study is likely due to the location of the reference air temperature measurement in the center of the gap, while the subcanopy air temperature and subsequently the canopy surface temperature remained warmer due to reduced radiative losses. The use of an offset is therefore suitable in environments where nighttime subcanopy air temperatures and canopy temperature remain warmer than the reference air temperature used for modeling.

Bulk offsets between air and canopy temperatures have been previously applied in a theoretical model by *Seyednasrollah et al*. [2013] using the canopy and tree trunk point measurements from *Pomeroy et al*. [2009]. Offsets in the study by *Seyednasrollah et al*. [2013] ranged between 0.5°C (dense canopies) and 1.5°C (sparse forests), smaller than those applied in this study. *Seyednasrollah et al*. [2013] applied offsets of 10°C to tree trunk temperatures in dense forests, which were not seen in the tree trunk measurements in the small gap and shaded side of the large gap, where tree trunk temperatures were between 4 and 5°C cooler than air temperature during the day. The differing results between studies and locations suggest that the selection of a bulk offset value is site or regionally specific and dependent on the location of reference air temperature measurements; i.e., an open site measurement could result in a different offset compared to an above-canopy measurement from a tower. Calculation of x is therefore likely a function of altitude, latitude, reference air temperature location, and tree species. While the constant bulk offset method can be applied in dense canopies at nighttime, this method to estimate canopy surface temperatures and subsequently subcanopy incoming longwave radiation is not suitable for application within sparse canopies exposed to direct incoming shortwave radiation where the offset between air and canopy temperatures is also dependent on canopy heating by shortwave radiation, which exhibits greater temporal and spatial variation.

Within the large gap, clear-sky and sunny conditions resulted in horizontal and vertical variations in canopy surface temperatures between 8 and 28°C, substantially higher than the 2–5°C variations in canopy surface temperatures in the small gap and in the large gap during cloudy conditions. Along the shaded edges of the large gap (south and east), vertical canopy temperature profiles showed warmer temperatures toward the top of the canopy, which was likely to be the result of solar heating from behind that does not penetrate to lower levels of the canopy. Additionally, tree trunk temperatures in the lower canopy had cooler temperatures than the remainder of the canopy. These vertical differences in canopy surface temperatures in the south and east further demonstrate the canopy acting as a cold sink due to the limited solar heating of both the air and canopy, i.e., leading to temperatures in the lower canopy that are cooler than in the upper canopy, shown by *Link and Marks* [1999] and in the air temperature data in *Webster et al*. [2016b].

Large differences in canopy surface temperatures were seen at the north and west edges of the large gap, i.e., in areas exposed to direct shortwave radiation. Thermal images showed that Sun-lit tree trunk temperatures increased up to 20°C above air temperature, and average canopy surface temperature (between 10 and 80% relative height) was warmer than reference air temperature. Consequently, modeling subcanopy longwave radiation using air temperature resulted in total seasonal RMSE at the north and west edges between 6.6 and 10.6 W m^{-2}, although individual bias errors were as high as 47 W m^{-2} during sunny conditions. The differences between calculated T_{eff} and T_{air} further demonstrated the increase in temperatures of solar heated canopies above local air temperature in *Pomeroy et al*. [2009] and *Webster et al*. [2016b]. Subsequently, air temperature is an incorrect representation of canopy surface temperatures within equation (1) in these Sun-lit environments under high solar angles. Importantly, it is in these areas of the subcanopy where melt initiates at the beginning of the season, therefore having substantial hydrological and ecological importance.

Air and canopy temperature measurements, as well as calculated T_{eff} values presented here demonstrate that modeling subcanopy incoming longwave radiation using a reference air temperature works sufficiently well most of the time. Nighttime periods and in areas with high subcanopy shortwave radiation, however, require corrections to reference air temperature to minimize model errors. Corrections for both these time periods

were applied using subcanopy shortwave radiation as a selection criteria for applying either a bulk offset or a multiple linear regression correction or simply applying reference air temperature (i.e., zero offset). Periods when air temperature would be a suitable predictor of canopy temperature during cloudy periods are also represented in this simple parameterization, where reduced subcanopy incoming shortwave radiation in normally sunny areas of the canopy drive the model to use air temperature instead of the multiple linear regression correction. The application of this correction parameterization can therefore be applied to a time series of air temperature and subcanopy shortwave radiation data to arrive at an estimate for subcanopy incoming longwave radiation. This was demonstrated in the improvement in subcanopy longwave radiation estimates at 20 different point locations across two snowmelt seasons in this study.

This improved model for calculating canopy temperatures throughout a subcanopy environment relies on meteorological parameters readily available to forest energy balance modelers. The use of a subcanopy shortwave radiation variable as opposed to an above-canopy variable incorporates the directional exposure of gap edges to shortwave radiation as well as the degree of penetration of shortwave radiation through the canopy in heterogeneous forests. Incorporation of these variables therefore allows the use of a simple V_f value as a canopy descriptor without any additional processing steps to take into account direction of exposure, computationally intensive canopy extinction coefficients or site-specific calibrations that do not take into account direction of exposure.

Coefficients within the correction parameterizations developed in this study, although site-specific, are expected to be applicable to further studies and models within environments with similar daily radiative regimes to Laret, i.e., European midlatitude alpine coniferous forests. However, within different forested environments or alpine regions with topographical shading, a site-specific calibration for the canopy temperature model is recommended. The correction parameterization developed within this study used data collected over a 24 h clear-sky period in a single location in the subcanopy and was successfully applied at all 20 radiometer locations across two snowmelt periods, reducing the mean bias and RMSE at all but two locations, where RMSE increased by less than 1 W m^{-2}. This simple calibration method, developed from data from a single radiometer pair, could easily be applied in other forested environments to better understand the relationship between canopy temperature and reference air temperature, thus simplifying data collection, calibration, and application.

This model is particularly suitable for simulation of subcanopy shortwave and longwave radiation at high spatial and temporal resolutions. Following initial calculation of sky-view fraction, the subsequent calculations to estimate subcanopy longwave radiation are relatively straightforward and less computationally intensive compared to process-based models [e.g., *Gouttevin et al*., 2015; *Broxton et al*., 2015]. The use of subcanopy shortwave radiation as a predictor variable is a value that is readily available in energy balance models, and the simple calibration procedure means that this model can be easily transferable to different altitudes and latitudes. This model is applicable within energy balance and snowmelt models where canopy structure descriptors can represent gap and edge environments within individual pixels or at subpixel resolution. It is therefore suitable to be used at a resolution that accurately represents forest discontinuities.

Using the parameterizations developed within this study, a model to calculate subcanopy incoming longwave radiation can therefore be applied at any location where V_f, reference air temperature, and subcanopy shortwave radiation information are available. Acquisition of high-resolution lidar data has facilitated the development of new methods making subcanopy shortwave radiation [*Musselman et al*., 2013] and canopy structure descriptors such as V_f [*Moeser et al*., 2014] readily available. An example of the combination of these methods to a wider scale was given at 2 m point spacing throughout the 170 × 220 m area surrounding the study site. The combination of the new parameterizations increased the representation of spatial and temporal variabilities in subcanopy longwave radiation around the discontinuous canopy environment. Noticeable improvements were along the edges of the large gap that showed increases in subcanopy longwave radiation that represented the movement of the Sun around the gap throughout the day. Longwave radiation hot spots were also better represented with the new parameterization, which therefore would further improve accurate estimation of snow disappearance dates along these discontinuities in canopy energy balance and snowmelt models applied at greater temporal scales. An improvement in the energy balance estimation below canopies would also help improve calculation and assessment of evapotranspiration rates, soil moisture distribution, and biological activity during and immediately following snowmelt periods,

in particular. Combined with a calculation of cloudiness for accurate continuous estimation of subcanopy shortwave radiation, the methods presented in this study would facilitate estimation of net radiation across landscape scales without requiring direct measurements of canopy temperatures or continuous measurements of subcanopy shortwave and longwave radiation.

7. Conclusions

This study demonstrated differences in thermal regimes around a large and small forest canopy gap using infrared thermal imagery. Five main canopy structure types were investigated: north edge (south facing, exposed), east edge (west facing, exposed), south edge (north facing, exposed), west edge (east facing, exposed), and small gap (shaded, closed). Vertical and horizontal variations in canopy surface temperatures along the edges of the large gap during sunny conditions were due to different directions of exposure of the canopy to direct shortwave radiation. In comparison, canopy surface temperature variations were relatively uniform in the small gap as well as during cloudy periods in both gaps, due to lack of exposure to direct shortwave radiation.

These measurements were used to develop a simple selection criteria for correcting reference air temperature for elevated canopy surface temperatures during (1) nighttime conditions where subcanopy shortwave radiation was 0 W m^{-2} and (2) periods of increased subcanopy shortwave radiation greater than 400 W m^{-2}. The use of subcanopy shortwave radiation better represents site or point-specific penetration of shortwave radiation through the canopy and is a value that is already readily available to energy balance and snowmelt modelers without an additional processing step for a site-specific extinction coefficient. The value of 400 W m^{-2} was selected, based on observations, to be representative of locations exposed to direct incoming shortwave radiation along forest gap edges and other discontinuous forest structures. Subcanopy shortwave and longwave radiation collected at a single point in the subcanopy over a 24 h clear-sky period was used to calculate a nighttime bulk offset of 3°C for scenario 1 and develop a multiple linear regression model for scenario 2 using reference air temperature and subcanopy shortwave radiation to predict canopy temperature with an RMSE of 0.7°C. When subcanopy shortwave radiation was between 1 and 400 W m^{-2}, reference air temperature (i.e., zero offset) was used to predict subcanopy incoming longwave radiation.

The incorporation of this improved method to estimate canopy temperature thus allowed for a simple estimation of subcanopy incoming longwave radiation around the subalpine field site. Modeling at 10 radiometer locations throughout two snowmelt seasons using these correction parameterizations reduced the mean bias and RMSE at all but two of the locations where RMSE remained within 1 W m^{-2}. Finally, the combination of this method with lidar data suggests potential for improved spatially distributed estimation of subcanopy net radiation across landscape scales.

Acknowledgments
Funding for the CMP3 and CGR3 radiometers used in this study was provided from the UK's Natural Environment Research Council (NERC) grant NE/H008187/1. The authors are grateful to the three reviewers for their suggestions and comments that helped improve the quality of the manuscript. Further data used in the analysis can be obtained by sending a written request to the first author (clare.webster@slf.ch) or the last author (jonas@slf.ch).

References

Anderson, M. C., R. G. Allen, A. Morse, and W. P. Kustas (2012), Use of Landsat thermal imagery in monitoring evapotranspiration and managing water resources, *Remote Sens. Environ.*, *122*, 50–65.

Ball, M., and H. Pinkerton (2006), Factors affecting the accuracy of thermal imaging cameras in volcanology, *J. Geophys. Res.*, *111*, B11203, doi:10.1029/2005JB003829.

Broxton, P. D., A. A. Harpold, J. A. Biederman, P. A. Troch, N. P. Molotch, and P. D. Brooks (2015), Quantifying the effects of vegetation structure on snow accumulation and ablation in mixed-conifer forests, *Ecohydrology*, *8*(6), 1073–1094.

Chen, J. M., and R. H. Zhang (1989), Studies on the measurements of crop emissivity and sky temperature, *Agric. For. Meteorol.*, *49*(1), 23–34.

Cohen, Y., V. Alchanatis, M. Meron, Y. Saranga, and J. Tsipris (2005), Estimation of leaf water potential by thermal imagery and spatial analysis, *J. Exp. Bot.*, *56*(417), 1843–1852.

Dozier, J., and S. G. Warren (1982), Effect of viewing angle on the infrared brightness temperature of snow, *Water Resour. Res.*, *18*, 1424–1434, doi:10.1029/WR018i005p01424.

Ellis, C. (2011), *Radiation and Snowmelt Dynamics in Mountain Forests*, Univ. of Saskatchewan, Saskatoon.

Essery, R., J. Pomeroy, C. Ellis, and T. Link (2008), Modelling longwave radiation to snow beneath forest canopies using hemispherical photography or linear regression, *Hydrol. Processes*, *22*(15), 2788–2800.

Gago, J., C. Douthe, R. E. Coopman, P. P. Gallego, M. Ribas-Carbo, J. Flexas, J. Escalona, and H. Medrano (2015), UAVs challenge to assess water stress for sustainable agriculture, *Agric. Water Manage*, *153*, 9–19.

Gouttevin, I., M. Lehning, T. Jonas, D. Gustafsson, and M. Mölder (2015), A two-layer canopy model with thermal intertia for an improved snowpack energy balance below needleleaf forest (model SNOWPACK, version 3.2.1, revision 741), *Geosci. Model Dev.*, *8*(8), 2379–2398.

Howard, R., and R. Stull (2013), IR radiation from trees to a ski run: A case study, *J. Appl. Meteorol. Climatol.*, *52*(7), 1525–1539.

Lawler, R. R., and T. E. Link (2011), Quantification of incoming all-wave radiation in discontinuous forest canopies with application to snowmelt prediction, *Hydrol. Processes*, *25*(21), 3322–3331.

Link, T. E., and D. Marks (1999), Point simulation of seasonal snow cover dynamics beneath boreal forest canopies, *J. Geophys. Res.*, *104*, 27,841–27,857, doi:10.1029/1998JD200121.

Liston, G. E., and K. Elder (2006), A distributed snow-evolution modeling system (SnowModel), *J. Hydrometeorol.*, *7*(6), 1259–1276.
Lundquist, J. D., S. E. Dickerson-Lange, J. A. Lutz, and N. C. Cristea (2013), Lower forest density enhances snow retention in regions with warmer winters: A global framework developed from plot-scale observations and modeling, *Water Resour. Res.*, *49*(10), 6356–6370, doi:10.1002/wrcr.20504.
Moeser, D., J. Roubinek, P. Schleppi, F. Morsdorf, and T. Jonas (2014), Canopy closure, LAI and radiation transfer from airborne LiDAR synthetic images, *Agric. For. Meteorol.*, *197*, 158–168.
Molotch, N. P., P. D. Brooks, S. P. Burns, M. Litvak, R. K. Monson, J. R. McConnell, and K. Musselman (2009), Ecohydrological controls on snowmelt partitioning in mixed-conifer sub-alpine forests, *Ecohydrology*, *2*(2), 129–142.
Musselman, K. N., S. A. Margulis, and N. P. Molotch (2013), Estimation of solar direct beam transmittance of conifer canopies from airborne LiDAR, *Remote Sens. Environ.*, *136*, 402–415.
Musselman, K. N., J. W. Pomeroy, and T. E. Link (2015), Variability in shortwave irradiance caused by forest gaps: Measurements, modelling, and implications for snow energetics, *Agric. For. Meteorol.*, *207*, 69–82.
Norman, J. M., and F. Becker (1995), Terminology in thermal infrared remote sensing of natural surfaces, *Remote Sens. Rev.*, *12*(3–4), 159–173.
Pomeroy, J. W., D. Marks, T. Link, C. Ellis, J. Hardy, A. Rowlands, and R. Granger (2009), The impact of coniferous forest temperature on incoming longwave radiation to melting snow, *Hydrol. Processes*, *23*(17), 2513–2525.
Reid, T., and R. Essery (2013), New methods to quantify canopy structure of leafless boreal birch forest from hemispherical photographs, *Open Journal of Forestry*, *3*, 70.
Rutter, N., et al. (2009), Evaluation of forest snow processes models (SnowMIP2), *J. Geophys. Res.*, *114*, D06111, doi:10.1029/2008JD011063.
Seyednasrollah, B., and M. Kumar (2013), Effects of tree morphometry on net snow cover radiation on forest floor for varying vegetation densities, *J. Geophys. Res. Atmos.*, *118*, 12,508–512,521, doi:10.1002/2012JD019378.
Seyednasrollah, B., and M. Kumar (2014), Net radiation in a snow-covered discontinuous forest gap for a range of gap sizes and topographic configurations, *J. Geophys. Res. Atmos.*, *119*, 10,323–10,342, doi:10.1002/2014JD021809.
Seyednasrollah, B., M. Kumar, and T. E. Link (2013), On the role of vegetation density on net snow cover radiation at the forest floor, *J. Geophys. Res. Atmos.*, *118*, 8359–8374, doi:10.1002/jgrd.50575.
Sicart, J. E., R. L. H. Essery, J. W. Pomeroy, J. Hardy, T. Link, and D. Marks (2004), A sensitivity study of daytime net radiation during snowmelt to forest canopy and atmospheric conditions, *J. Hydrometeorol.*, *5*(5), 774–784.
Sobrino, J. A., and J. Cuenca (1999), Angular variation of thermal infrared emissivity for some natural surfaces from experimental measurements, *Appl. Opt.*, *38*(18), 3931–3936.
Thimonier, A., I. Sedivy, and P. Schleppi (2010), Estimating leaf area index in different types of mature forest stands in Switzerland: A comparison of methods, *Eur. J. For. Res.*, *129*, 543–562.
Webster, C., N. Rutter, F. Zahner, and T. Jonas (2016a), Measurement of incoming radiation below forest canopies: A comparison of different radiometer configurations, *J. Hydrometeorol.*, *17*(3), 853–864.
Webster, C., N. Rutter, F. Zahner, and T. Jonas (2016b), Modeling subcanopy incoming longwave radiation to seasonal snow using air and tree trunk temperatures, *J. Geophys. Res. Atmos.*, *121*, 1220–1235, doi:10.1002/2015JD024099.
Zehe, E., and G. Blöschl (2004), Predictability of hydrologic response at the plot and catchment scales: Role of initial conditions, *Water Resour. Res.*, *40*, W10202, doi:10.1029/2003WR002869.